Journal of
Polymer & Composites
https://journals.stmjournals.com/jopc

ISSN: 2321-2810 (Online)
ISSN: 2321-8525 (Print)
Volume 14, Special Issue 1, 2026
DOI (Journal): 10.37591/JoPC

Research JoPC

MHD-Assisted Flow Regulation of Viscoelastic Polymer Fluids for Industrial Cooling and Composite Fabrication with Isotherml Plates

M. Siva Sankar Reddy[1], K. Venkateswara Raju[2], B. Hari Babu[3], Y. Satheesh Kumar Reddy[4], Madhumohana Raju A. B.[5,*]

Abstract

This study investigates the magnetohydrodynamic (MHD) regulation of viscoelastic polymer fluid flow over a permeable plate, emphasizing its relevance to industrial cooling and composite fabrication. An incompressible, electrically conducting viscoelastic fluid is analyzed under a transverse magnetic field with Hall and ion-slip effects to capture electromagnetic alterations in polymer transport. The governing non-dimensional equations for momentum, temperature, and concentration are solved analytically using the perturbation method. The results show that increasing magnetic field strength suppresses primary velocity due to Lorentz resistance, enabling effective control during polymer cooling, while Hall and ion-slip parameters enhance both primary and secondary flow components, improving resin dispersion in composite processing. Temperature decreases with higher Prandtl number and radiation absorption, indicating improved thermal regulation. Quantified variations in skin friction, Nusselt number, and Sherwood number further reveal the combined influence of electromagnetic and viscoelastic parameters on heat and mass transfer. These findings provide practical insights for optimizing polymer flow behavior and enhancing efficiency in advanced manufacturing applications

Keywords: Viscoelastic polymer fluid; Hall effect; Ion-slip effect; Permeable plate; Industrial cooling; Composite fabrication; Perturbation method; Electromagnetic flow control.

***Author for Correspondence**
Madhumohana Raju A.B.

[1]Assistant Professor, Department of Humanities and Basic Séances, G. Pulla Reddy Engineering College (Autonomous), Kurnool, Andhra Pradesh, India
[2]Professor, Department of Mathematics, Sri Venkateswara College of Engineering (Autonomous), Tirupati, Andhra Pradesh, India
[3]Assistant Professor, Department of Mathematics, PACE Institute of Technology & Sciences (Autonomous), Ongole, Andhra Pradesh, India
[4]Assistant Professor, Department of Humanities and Sciences (Mathematics), K. S. R. M. College of Engineering (Autonomous), Kadapa, Andhra Pradesh, India
[5]Associate Professor, Department of Mathematics, New Horizon College of Engineering, Bangalore, Karnataka, India

Received Date: 20 November 2025
Accepted Date: 14 December 2025
Published Date: 20 January 2026

Citation: M. Siva Sankar Reddy, K. Venkateswara Raju, B. Hari Babu, Y. Satheesh Kumar Reddy, Madhumohana Raju A.B. MHD-Assisted Flow Regulation of Viscoelastic Polymer Fluids for Industrial Cooling and Composite Fabrication with Isotherml Plates. Journal of Polymer & Composites. 2026; 14(Special Issue 1): S851–S866p.

INTRODUCTION

Non-Newtonian viscoelastic polymer fluids are widely used in polymer extrusion, industrial cooling, composite fabrication, and electrically controlled processing due to their ability to exhibit both elastic and shear-dependent viscous behaviour. Their transport characteristics become even more significant when influenced by magnetic fields, porous structures, and cross-diffusion mechanisms. Revathi *et al.* [1] demonstrated how cross-diffusion, couple-stress and non-Fourier heat flux strongly affect hybrid nanofluid behaviour in thermally sensitive polymer systems. Yadav *et al*. [2] showed that temperature-dependent viscosity and thermal conductivity substantially modify convection patterns in Jeffrey fluids within porous rotating layers. Kommaddi, Raghunath and co-authors [3] analysed Hall current, Dufour and radiation absorption effects on unsteady MHD rotating flows, emphasizing their relevance in electrically assisted polymer processing. Similarly, Kodi *et al*. [4] reported the impact of MHD, radiation absorption and diffusion-thermo effects on Jeffrey nanofluid flow over inclined surfaces. Raghunath and collaborators further explored Hall current, Soret effects and thermal radiation in porous MHD flows of Jeffrey fluids [5–7], highlighting their importance in heat transfer enhancement during composite curing. Maatoug *et al*. [8] examined Darcy–Forchheimer drag, chemical species variation and viscous dissipation in Jeffrey nanofluids, revealing their significance in squeezing-flow-based polymer and composite manufacturing. Collectively, these studies confirm that MHD-assisted regulation of viscoelastic polymer fluids provides effective control for industrial cooling, composite fabrication, and advanced thermal-processing applications.

Hall and ion-slip effects play a significant role in magnetohydrodynamic (MHD) flows of electrically conducting polymeric and non-Newtonian fluids, especially under strong magnetic fields where charge separation becomes prominent. These effects modify current density distribution, induce secondary velocities, and alter Lorentz forces, making them essential for accurate modelling in polymer cooling, composite fabrication, electromagnetic pumping, and thermomechanical processing. Katikala *et al*. [9] showed that Hall current, radiation absorption, and diffusion-thermo interactions strongly influence second-grade fluid motion in porous media with Joule heating and viscous dissipation. Prasad *et al*. [10] demonstrated that Hall current and thermal diffusion significantly modify the rotating MHD flow of Cu–TiO_2 nanofluids under thermal radiation and chemical reaction. Raghunath *et al*. [11] highlighted the importance of Hall and ion-slip effects in mixed convective Casson fluid flow past inclined porous plates under radiation absorption and diffusion-thermo influences. Sunitha Rani *et al*. [12] emphasized that Joule heating, thermal radiation, and Hall current dramatically alter unsteady rotating MHD flow behaviour. Raghunath *et al*. [13] further explored Hall-driven modifications in hybrid nanofluid transport with internal heat absorption. Ramachandra Reddy *et al*. [14] incorporated Hall current, activation energy, and thermo-diffusion effects into Darcy–Forchheimer nanofluid models, demonstrating substantial changes in temperature and concentration fields. Raghunath *et al*. [15] studied Hall, ion-slip, diffusion-thermo, and radiation absorption effects in unsteady MHD flows through porous media. Kumar *et al*. [16] investigated Casson nanofluids with activation energy, Hall current, and thermal radiation, confirming strong Hall-induced modifications. Omar *et al*. [17] reported that Hall current and Soret effects significantly change second-grade fluid behaviour under thermal radiation and chemical reactions. Deepthi *et al*. [18] provided recent developments on Hall, ion-slip, and thermo-diffusion impacts in radiative second-grade materials relevant to micromachine applications. Aruna *et al*. [19] also confirmed that radiation absorption, Hall current, and ion-slip interactions markedly alter unsteady second-grade fluid flow through porous media. Collectively, these studies demonstrate that Hall and ion-slip effects are essential for accurate modelling of MHD-assisted viscoelastic polymer flows used in industrial cooling, composite fabrication, and electromagnetic processing systems.

Magnetohydrodynamics (MHD), the study of electrically conducting fluid motion under magnetic fields, plays a fundamental role in controlling heat and mass transfer in polymer processing, composite fabrication, nanofluid-based cooling, metallurgical operations, and energy systems. The application of magnetic fields introduces Lorentz forces that regulate boundary-layer behaviour, enhance or suppress convection, and significantly influence entropy generation and thermal performance. Suneetha *et al*. [20] optimized entropy generation in hybrid nanofluids using non-Fourier heat flux and confirmed that MHD effects strongly alter thermal transport. Jyothi *et al*. [21] used neural-network modelling to show that magnetic fields enhance boundary-layer stability in Sisko nanofluids. Bin Zafar *et al*. [22] demonstrated how Lorentz forces modify Prandtl fluid transport along stretching cylinders, relevant for composite coating processes. Viswanath *et al*. [23] highlighted the influence of radiant heating on unsteady MHD hybrid nanofluid flow. Lavanya *et al*. [24] found that MHD control improves thermal stability in Carreau nanofluids. Pasha *et al*. [25] analysed rotational and thermal diffusion effects in viscoelastic MHD flows through porous media, while Ramachandra Reddy *et al*. [26] examined magnetic-field alignment effects on Casson convection with Joule heating. Hussain *et al*. [27] studied three-dimensional hybrid nanofluid MHD flows for enhanced heat transfer. Valiveti *et al*. [28]

investigated heat and mass transfer in unsteady MHD Casson fluids under thermal diffusion and heat source conditions. Jyothi *et al*. [29] further demonstrated the role of MHD in SWCNT nanofluid radiation transport. Bhargava *et al*. [30] analysed mixed convection in rotating 3D hybrid nanofluids in porous media. Raghunath *et al*. [31] assessed buoyancy and thermodynamic effects of nanoparticles in engine oil under magnetic influences. Zhang *et al*. [32] studied 3D-MHD Maxwell fluids with thermo-diffusion and activation energy. Yadav *et al*. [33] examined rotation and variable conductivity in Casson convection with MHD effects. Finally, Sridevi *et al*. [34] explored thermal radiation and chemical reaction influences on MHD hybrid nanofluid flow through porous media. Collectively, these studies establish MHD as a powerful mechanism for controlling viscoelastic, polymeric, and nanofluid transport in advanced thermal and composite manufacturing systems.

The novelty of this study lies in its application-oriented investigation of MHD-assisted regulation of viscoelastic polymer fluid flow, specifically targeting industrial cooling and composite fabrication processes. Unlike traditional MHD analyses, this work simultaneously incorporates both Hall current and ion-slip effects, providing a deeper understanding of their combined influence on primary and secondary flow characteristics over a permeable plate. The analytical perturbation solution offers closed-form expressions that enhance physical interpretation and complement numerical methods commonly used in similar studies. Additionally, the comprehensive evaluation of heat and mass transfer parameters including skin friction, Nusselt number, and Sherwood number reveals new insights into electromagnetic control mechanisms applicable to polymer extrusion and composite curing. By establishing how magnetic intensity and cross-electromagnetic interactions can be used as tunable parameters to optimize thermal and solutal transport, the study bridges theoretical fluid dynamics with practical needs in advanced polymer and composite engineering.

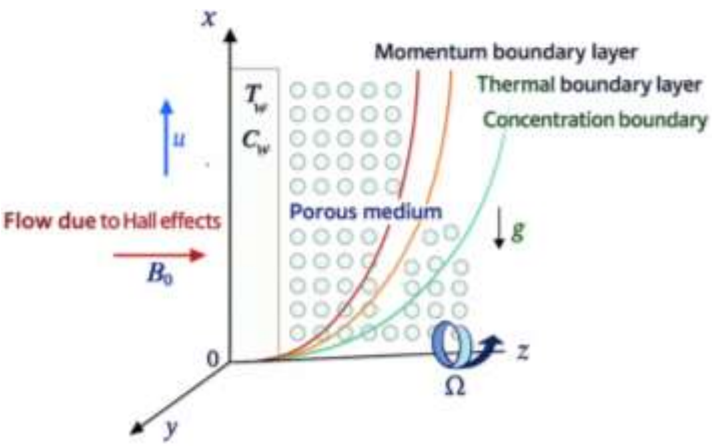

Figure 1. Physical configuration of the phenomena.

MATHEMATICAL FORMULATION

The present study analyzes the MHD-assisted flow regulation of a viscoelastic polymer fluid over a vertical permeable plate embedded in a porous medium, incorporating the combined influences of Hall and ion-slip effects as illustrated in Fig. 1. The plate is maintained at constant wall temperature T_w and concentration C_w, while a uniform transverse magnetic field B_0 is applied normal to the flow. Under strong magnetic fields, charge separation generates a Lorentz force that induces a secondary flow in the y-direction, producing the Hall-driven motion shown in the figure. Ion-slip further modifies the effective current density and alters electromagnetic resistance. The viscoelastic nature of the polymer fluid is captured using an appropriate constitutive relation, while the porous medium introduces Darcy–Forchheimer resistance to momentum transport. As shown, the momentum, thermal, and concentration boundary layers develop away from the plate, influenced by buoyancy forces acting downward. The coordinate system is chosen such that xxx is normal to the plate, y is tangential to the flow direction, and z accounts for rotational or secondary effects. Considering these physical assumptions, the governing equations for continuity, momentum, energy, and concentration are formulated by including magnetic forces, Hall and ion-slip corrections, viscous dissipation, Joule heating, and porous medium drag. These partial differential equations are transformed into a system of nonlinear ordinary differential equations using similarity transformations, and solved analytically through the perturbation method to obtain the velocity, temperature, and concentration distributions relevant to industrial cooling and composite fabrication applications.

The liquid of fluid via permeable media in a rotating channel is regulated by the following equation when using the Boussinesq approximation

$$\frac{\partial u}{\partial x}+\frac{\partial u}{\partial y}=0 \tag{1}$$

$$\left(1+\lambda\frac{\partial}{\partial t}\right)\frac{\partial q}{\partial t}+w\frac{\partial q}{\partial z}=-\left(1+\lambda\frac{\partial}{\partial t}\right)\frac{1}{\rho}\frac{\partial p}{\partial x}+v\frac{\partial^2 q}{\partial z^2}+\left(1+\lambda\frac{\partial}{\partial t}\right)\frac{\sigma B_0^2(\alpha_2 v-\alpha_1 u)}{\rho}-\frac{v}{k}q+g\beta(T-T_\infty)+g\beta^*(C-C_\infty) \tag{2}$$

$$\frac{\partial T}{\partial t}+w\frac{\partial T}{\partial z}=\frac{k_1}{\rho C_p}\frac{\partial^2 T}{\partial z^2}-\frac{Q_0}{\rho C_p}(T-T_\infty)+Q_1(C-C_\infty) \tag{4}$$

$$\frac{\partial C}{\partial t}+w\frac{\partial C}{\partial z}=D\frac{\partial^2 C}{\partial z^2}-K_c(C-C_\infty) \tag{5}$$

Under the assumptions stated above, the following equations provide the relevant limit circumstances for the velocity, temperature, and concentration distributions.

$$u=0, v=0, T>T_\infty, C>C_\infty, t \le 0 \text{ for all } z \tag{6}$$

$$u=U_0, v=0, T=T_w, C=C_{w,}\ t>0, \text{ at } z=0 \tag{7}$$

$$u\to 0, v\to 0, T\to T_\infty C\to C_\infty, \text{ as } z\to\infty \tag{8}$$

w is either an invariant or a part of time, according to the solution to the equation of continuity; hence, we assume that

$$w = - w^1{}_0 \tag{9}$$

Outside the boundary layer, Equation (2) gives

$$-\left(1+\lambda\frac{\partial}{\partial t}\right)\frac{1}{\rho}\frac{\partial p*}{\partial x*}=\frac{\partial U_\infty}{\partial t*}+\frac{v}{k^*}U_\infty^*+\left(1+\lambda\frac{\partial}{\partial t}\right)\left(\frac{\sigma B_0^2}{\rho}U_\infty^* Sin^2\gamma\right) \tag{10}$$

We familiarise the non-dimensional portions and specifications listed below to normalise the mathematical model of the physical situation.

$$q*=\frac{q}{w_0}, w*=\frac{w}{w_0}, z^*=\frac{w_0 z}{v}, U_0^*=\frac{U_0}{w_0}, U_\infty^*=\frac{U_\infty}{w_0}, t^*=\frac{t w_0^2}{v}, \theta=\frac{T-T_\infty}{T_w-T_\infty}, \varphi=\frac{C-C_\infty}{C_w-C_\infty},$$
$$M^2=\frac{\sigma B_0^2 v}{\rho w_0^2}, Pr=\frac{v\rho C_p}{k_1}=\frac{v}{\alpha}, Sc=\frac{v}{D}, Gr=\frac{vg\beta(T_w-T_\infty)}{w_0^3}, Gm=\frac{vg\beta^*(C_w-C_\infty)}{w_0^3},$$
$$K=\frac{w_0^2 k}{v^2}, H=\frac{vQ_0}{\rho C_p w_0^2}, K_c=\frac{K_c v}{w_0^2}, Q_1=\frac{vQ_1(C_w-C_\infty)}{(T_w-T_\infty)w_0^2}, \eta=\frac{\lambda v_0^2}{\vartheta} \tag{11}$$

Using non-dimensional components, the system of equations (2)-(5) may be condensed to the following:

$$\left(1+\eta\frac{\partial}{\partial t}\right)\frac{\partial q}{\partial t}-\frac{\partial q}{\partial z}=\left(1+\eta\frac{\partial}{\partial t}\right)\frac{dU_\infty}{dt}+\frac{\partial^2 q}{\partial z^2}-\left(1+\eta\frac{\partial}{\partial t}\right)M^2(\alpha_1+i\alpha_2)qSin^2\gamma+Gr\theta+Gm\rightleftarrows\varphi \tag{12}$$

$$\frac{\partial\theta}{\partial t}-\frac{\partial\theta}{\partial z}=-\frac{1}{Pr\frac{\partial^2\theta}{\partial z^2}} \tag{13}$$

$$\frac{\partial\varphi}{\partial t}-\frac{\partial\varphi}{\partial z}=\frac{1}{Sc}\frac{\partial^2\varphi}{\partial z^2}-K_c\varphi \tag{14}$$

The limit circumstances that resemble to this condition are furnished by

$$q=u_0,\theta=1,\varphi=1 \text{ at } z=0 \tag{15}$$

$$q=0,\theta\to 0,\varphi\to 0 \text{ as} z\to\infty \tag{16}$$

SOLUTION OF THE PROBLEM

This can be accomplished by reducing the partial differential equations in closed form to a collection of ordinary differential equalizations in the dimensionless form that can be translated analytically. The following equations describe the variables defining the velocity, temperature, and concentration:

$$q=q_0(z)+E_cq_1(z)+O(E_c^2) \tag{17}$$

$$\theta=\theta_0(z)+E_c\theta_1(z)+O(E_c^2) \tag{18}$$

$$\phi=\phi_0(z)+E_c\phi_1(z)+O(E_c^2) \tag{19}$$

Using the equations (17-19), into the eqns (12-14), and combining the harmonic and non-harmonic terms, the ignoring more heightened order terms of an equation (12-14), one gets the following sets of equations: $(q_0,\theta_0,\phi_0)and(q_1,\theta_1,\phi_1)$,

$$\frac{\partial^2 q_0}{\partial z^2}+\frac{\partial q_0}{\partial z}-M^2(\alpha_1+i\alpha_2)q_0=-Gr\theta_0-Gm \rightleftarrows \varphi_0 \tag{20}$$

$$\frac{\partial^2\theta_0}{\partial z^2}+Pr\frac{\partial\theta_0}{\partial z}-H\,Pr\,\theta_0=-Q_1\,Pr\rightleftarrows\varphi_0 \tag{21}$$

$$\frac{\partial^2\varphi_0}{\partial z^2}+Sc\frac{\partial\varphi}{\partial z}-ScKc\varphi_0=0 \tag{22}$$

$$\frac{\partial^2 q_1}{\partial z^2}+\frac{\partial q_1}{\partial z}-M^2(\alpha_1+i\alpha_2)(1+\eta)q_1=-Gr\theta_1-Gm\rightleftarrows\varphi_1-Aq_0^{\iota}-(1+\eta)(\xi+n) \tag{23}$$

$$\frac{\partial^2\theta_1}{\partial z^2}+Pr\frac{\partial\theta_1}{\partial z}-H\,Pr\,\theta_1=-Q_1\varphi_1\,Pr\rightleftarrows \tag{24}$$

$$\frac{\partial^2\varphi_1}{\partial z^2}+Sc\frac{\partial\varphi_1}{\partial z}-K_cSc\varphi_1=0 \tag{25}$$

The boundary conditions that relate to this are as follows:

$$q_0=U_0,q_1=0,\theta_0=1,\theta_1=1,\varphi_0=1,\varphi_1=0 \text{ at } z=0 \tag{26}$$

$q_0=0,q_1=0,\theta_0=0,\theta_1=0,\varphi_0=0,\varphi_1=0$ as $z\to\infty$ (34)

Equations with substitutions (20)– (26) We derive the velocity temperature and concentration field from equations (17-19).

$q=b_9\,exp(-m_3z)+b_{10}\,exp(-m_1z)+b_{11}\,exp(-m_5z)+Ec(b_{12}\,exp(-m_4z)+b_{13}\,exp(-m_3z)+b_{14}\,exp(-m_1z)+b_{15}\,exp(-m_2z)+b_{16}\,exp(-m_5z)+b_{17}\,exp(-m_6z))$ (27)

$$\theta=b_3\,exp(-m_3z)+b_4\,exp(-m_1z)+Ec(b_5\,exp(-m_3z)+b_6\,exp(-m_1z)+b_7\,exp(-m_2z)+b_8\,exp(-m_4z)) \tag{28}$$

$$\varphi=exp(-m_1z)\rightleftarrows+Ec(b_3\,exp(-m_3z)+b_4\,exp(-m_1z)) \tag{29}$$

The following are some examples of how these parameters may be specified and calculated.

$$\tau=\left(\frac{\partial q}{\partial z}\right)_{z=0}=-(b_9m_3+b_{10}m_1+b_{11}m_5)-Ec(b_{12}m_4+b_{13}m_3+b_{14}m_1+b_{15}m_2+b_{16}m_5+b_{17}m_6)$$

$$Nu = -\left(\frac{\partial\theta}{\partial z}\right)_{z=0} = b_3 em_3 + b_4 m_1 z + Ec(b_5 em_3 + b_6 m_1 + b_7 m_2 + b_8 m_4)$$

$$Sh = -\left(\frac{\partial\varphi}{\partial z}\right)_{z=0} = m_1 + Ec(b_3 m_3 + b_4 m_1)$$

RESULTS AND DISCUSSION

With this work, the outcomes of radiation absorption Hall and ion slip of unstable free convective gush of a dense incompressible electrically manipulating liquid across an unbounded upright permeable platter under the impact of an invariant transverse magnetic domain are investigated in more detail. The regular perturbation strategy is exploited to translate the governing equalizations of the flow field when the Eckert number Ec is minimal. Analysis has been used to derive closed-form solutions for the variables of velocity, temperature, and concentration. The computational behaviour of these solutions has been discussed concerning various flow specifications such as the Magnetic field (M), Hall specification (βe), ion slip specification (βi), thermal Grashof numeral (Gr), mass Grashof numeral (Gm), the permeability of porous media (K), radiation absorption specification (Q_1), the Prandtl numeral (Pr), Chemical Reaction specification (Kc), Heat origin specification (H). The velocity distributions are shown in figures 2-9, whereas the temperature and concentration distributions are depicted in figures 10-14. It is calculated numerically and examined with the governing specifications; the results are recorded in the following tables: stresses, Nusselt number, and Sherwood number at the plate (1-3).

Fig. 2 demonstrates the significance of the Magnetic domain specification M for the velocity segments u and v. Through a change in the magnetic domain specification M, the initial velocity segment u enriches while the secondary velocity segment v diminishes. As is anticipated, the expansion of M reduces the consequent velocity. Because of the classical outcome, the Lorentz force emerges from the magnetic domain's submission to an electrically conducting fluid, giving rise to a resistive form of pressure. Pertinent to this potency, the fluid flow's movement in the impetus border layer consistency begins to slow. On both the primary and secondary velocities, the influence of the visco-elastic fluid parameter was shown in Figure 3. In this case, it is shown that the visco-elastic fluid decreases as the principal velocity increases and the secondary velocity decreases. The demeanor of velocity exoneration with Hall and ion-slip characteristics was displayed in Figures 4 and 5. The initial velocity u enhances, whereas secondary velocity v diminishes with increasing Hall (βe) and ion slip (βi) variables across the fluid area. It's worth noting that the increased velocity and thickness of the momentum boundary layer across the liquid area is due to the strengthening of Hall and ion-slip characteristics. The addition of the Hall parameter reduces the effective conductibility, lowering the magnetic cruelness. In addition, as the ion-slip parameter is increased, the efficient conductivity rises, lowering the attenuation force and increasing velocity.

Fig. 6-7 shows the outcomes of thermal and solutal Grashof numerals on u and v. Increasing thermal Grashof numeral Gr and solutal Grashof numeral Gm increases primary velocity u and decreases secondary velocity v. Gr and Gm denote the proportion of buoyant thermal strength to thick hydrodynamic strength in the frontier layer, respectively. The intensification of heat and solutal buoyancy significances increases fluid velocity. The velocity distribution widens rapidly towards the permeable surface and decreases quickly for the viscous stream.

Figure 8 shows that as the permeability K expansions, the primary velocity segment u improves while the secondary velocity segment v declines. The main velocity component u contributes significantly to the Hall current effects over the fluid area. The bigger the quantity of K, the higher the consequent velocity and, as an outcome, the consistency of the momentum border layer. The fluid velocity is respected in the flow constituency occupied by the fluid at a lower velocity as the penetrability decreases. Figure 9 describes the consequence of the radiating absorption specification in both the primary and secondary velocity directions. The statistics show that the preliminary velocity graphs increase radiating absorptions, while the secondary velocity graphs decrease due to radiating across the fluid area. It was fascinating to see how an increase in the radiating absorption characteristics enhances the resulting velocity.

Figures 10-12 depicted the relationship between the temperature of the gush domain and the Prandtl numeral (Pr), heat conception specification (H), and radiation absorption specification (Q_1), respectively. Figure 10 demonstrates the influence of the Prandtl numeral (Pr) on temperature silhouettes in the existence of several liquids, including hydrogen (Pr = 0.684), air (Pr = 0.699), air (Pr = 0.72), and carbon dioxide (Pr = 0.76), among others. It can be seen in this image that improving the Prandtl numeral outcomes in decline in the temperature of the flow field at all places. This is compatible with the thickness of the thermal border layer diminishes as the Prandtl numeral gains. Figure 11, the temperature of the flow field is reduced when the heat source specification is enriched in value. This may occur as a result of the fluid's elastic nature. The outcomes of the radiation-absorption specification on temperature representations are discussed in detail inside the frontier layers of the model as shown in figure 12. It has become clear that temperature distributions increase radiation absorption functions as the radiation intensity increases.

Figures 13-14 illustrate the outcome of chemical response specification Kc, and the Schmidt number, on concentration distribution. Progress in the chemical response specification s seen in Figure 13. Kc rapidly depleted the concentration profiles. The concentration domain shrinks because the chemical reaction effects on the amounts of solutal particles increase as chemically responding parameters increase. As a result, the chemical reaction narrows the solute boundary stratum width. With improving Schmidt numeral Sc, the concentration disbandment at all sites of the gush domain diminishes, as seen in Figure 14. More rotund diffusing species have a more substantial retarding influence on the concentration disbandment of the flow domain, as shown by this experiment.

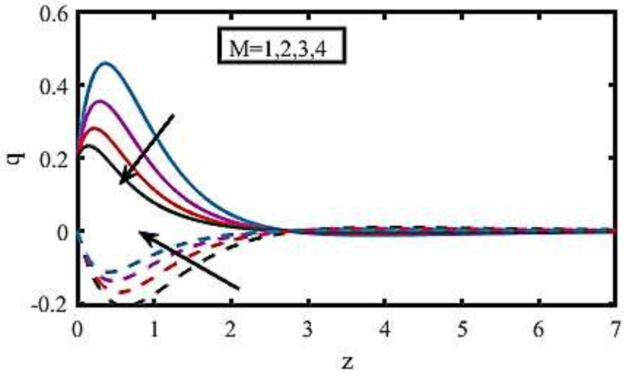

Figure 2. Velocity profiles for u and v for Magnetic field parameter (M)

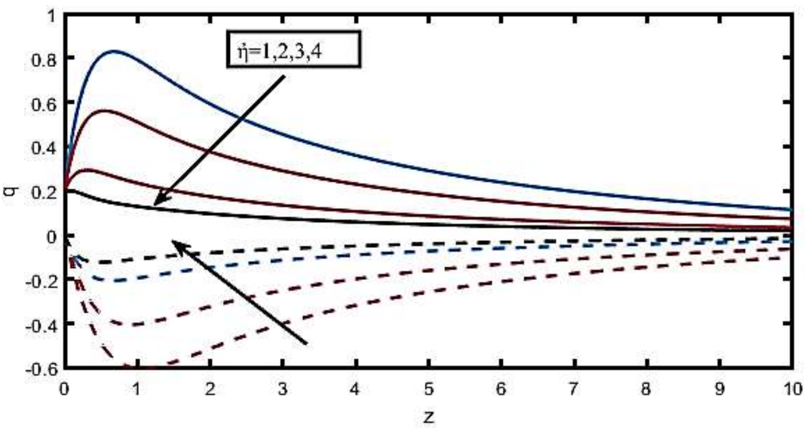

Figure 3. Velocity profiles for u and v for visco-elastic fluid parameter (ṅ)

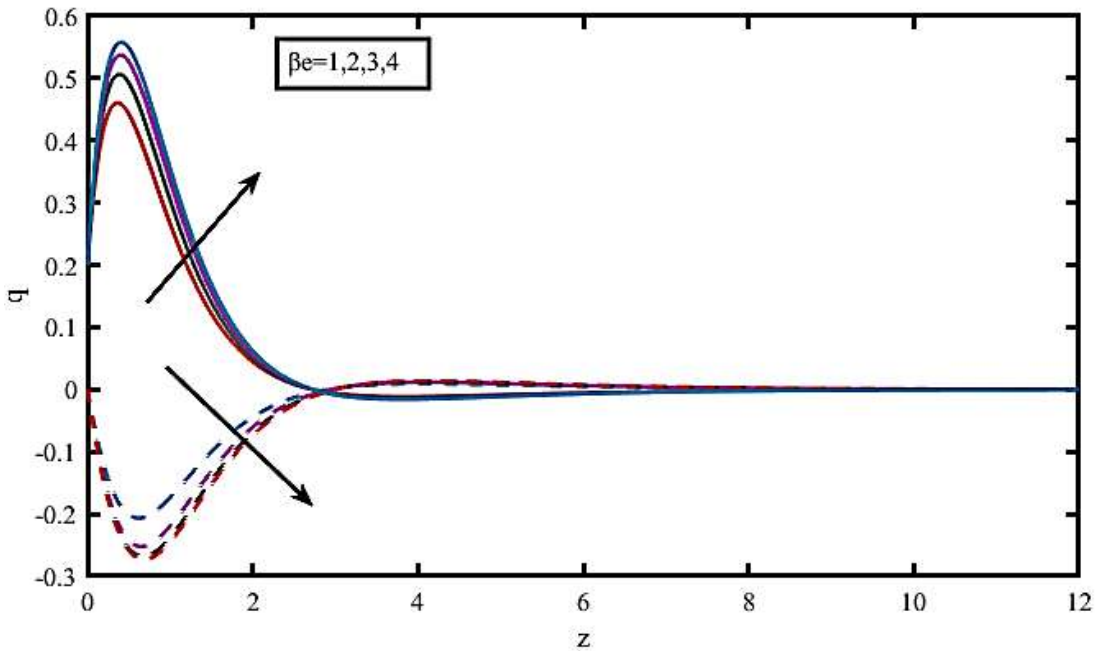

Figure 4. Velocity profiles for u and v for Hall parameter (β_e)

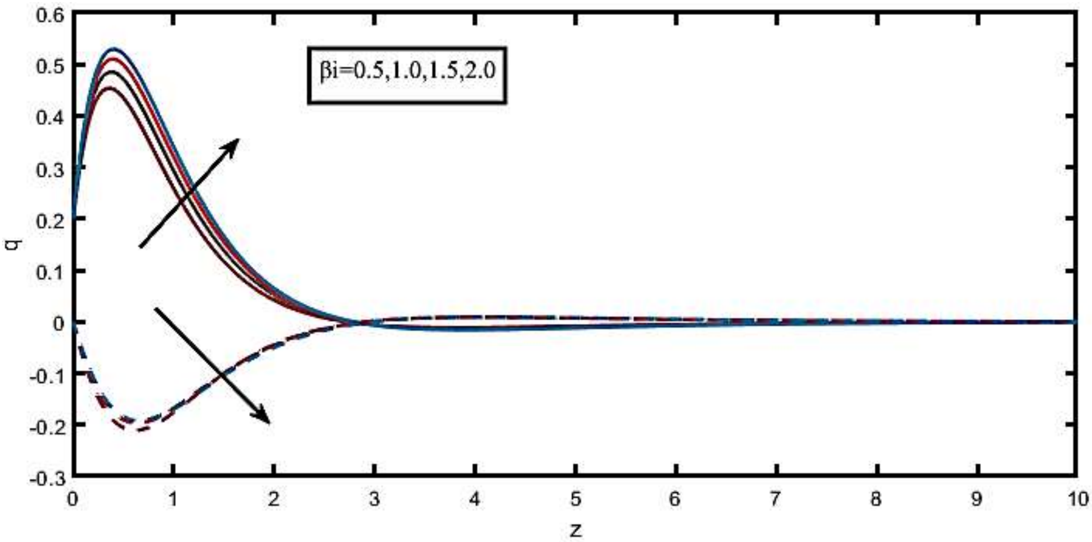

Figure 5. Velocity profiles for u and v for Hall parameter (β_i)

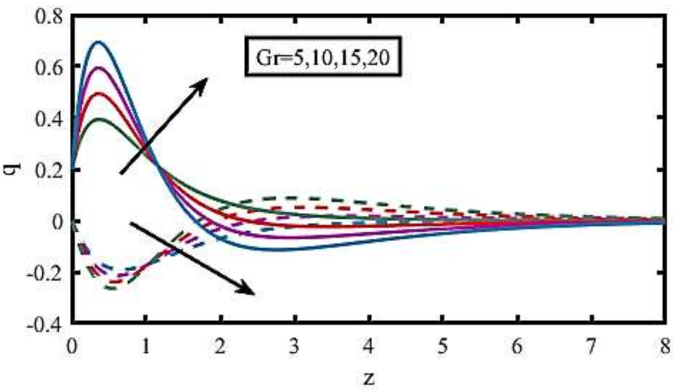

Figure 6. Velocity profiles for u and v for thermal Grashof number (Gr)

Journal of Polymer & Composites
Volume 14, Special Issue 1
ISSN: 2321-2810 (Online), ISSN: 2321-8525 (Print)

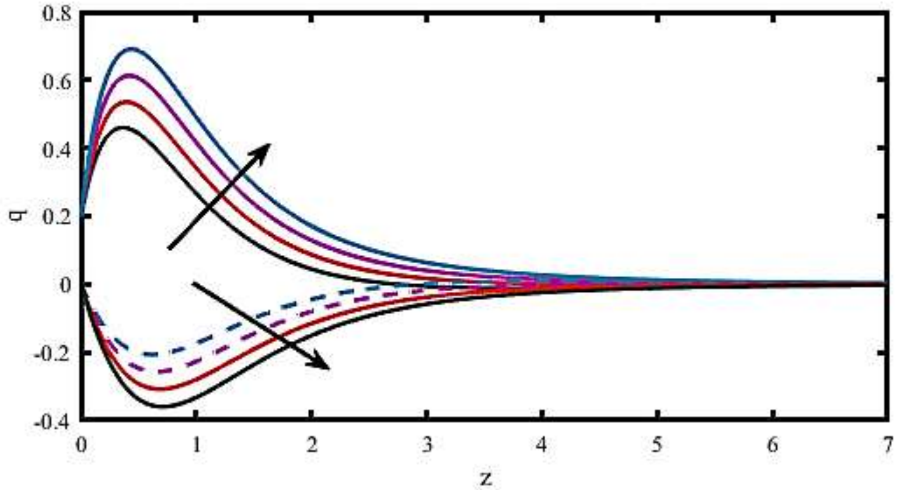

Figure 7. Velocity profiles for u and v for modified Grashof number (Gm)

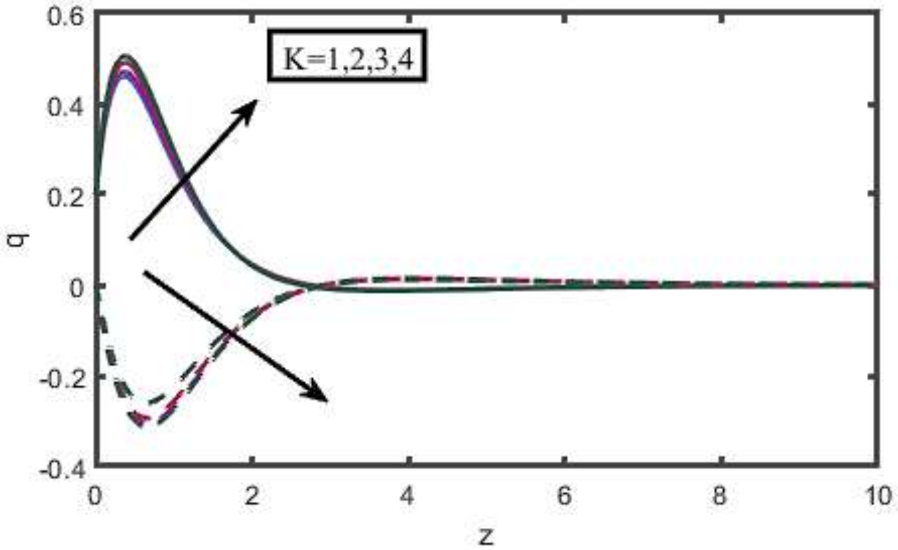

Figure 8. Velocity profiles for u and v for Permeability of porous media (K)

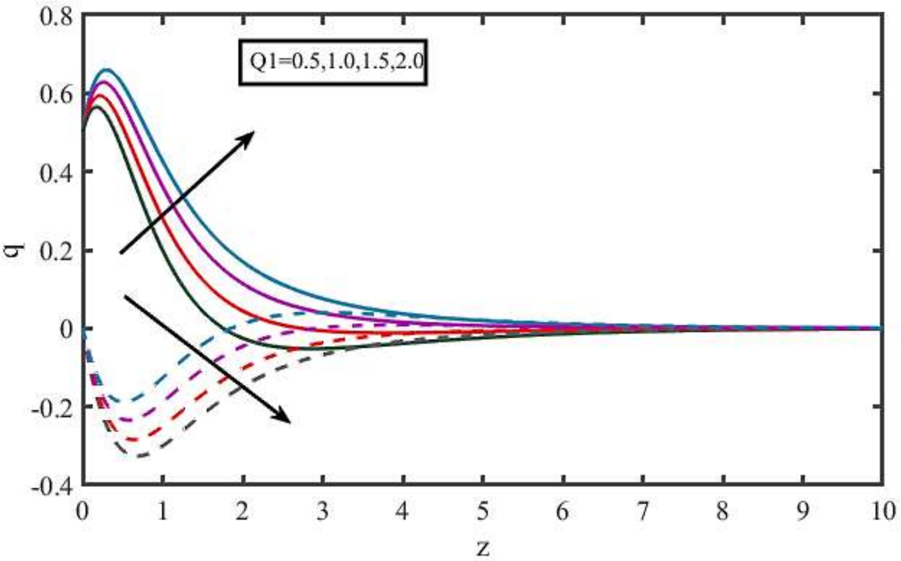

Figure 9. Velocity profiles for u and v for Radiation Absorption (Q_1)

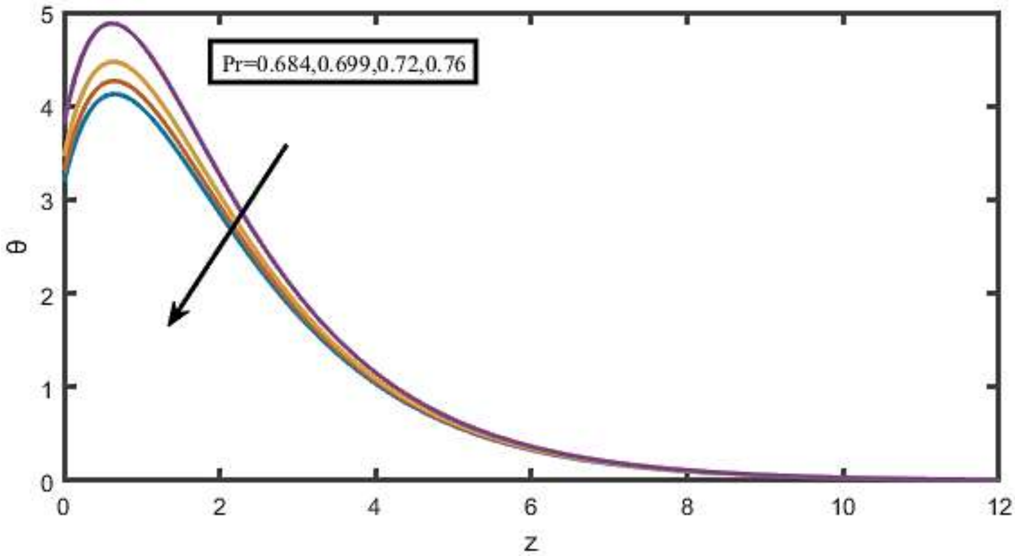

Figure 10. Temperature profiles for Prandtl number (Pr)

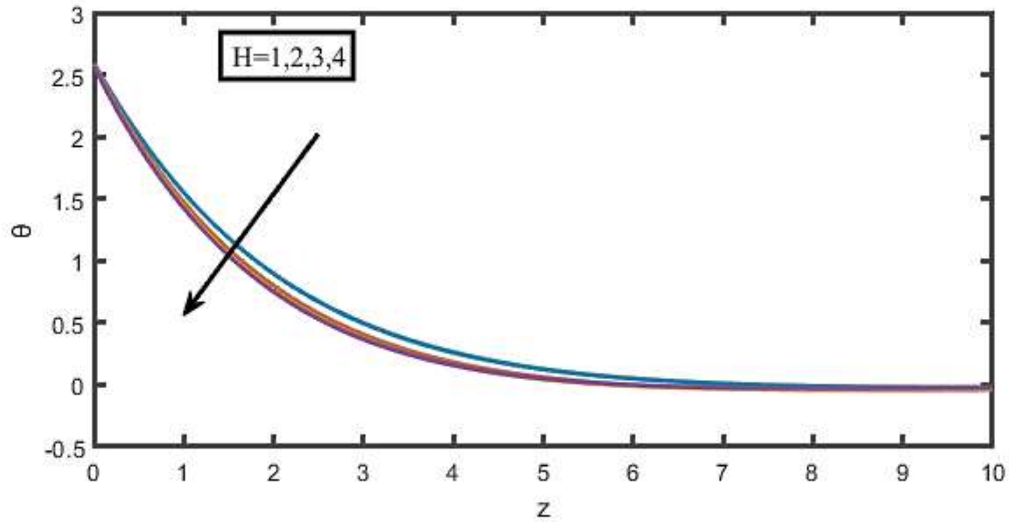

Figure 11. Temperature profiles for Heat absorption Parameter (H)

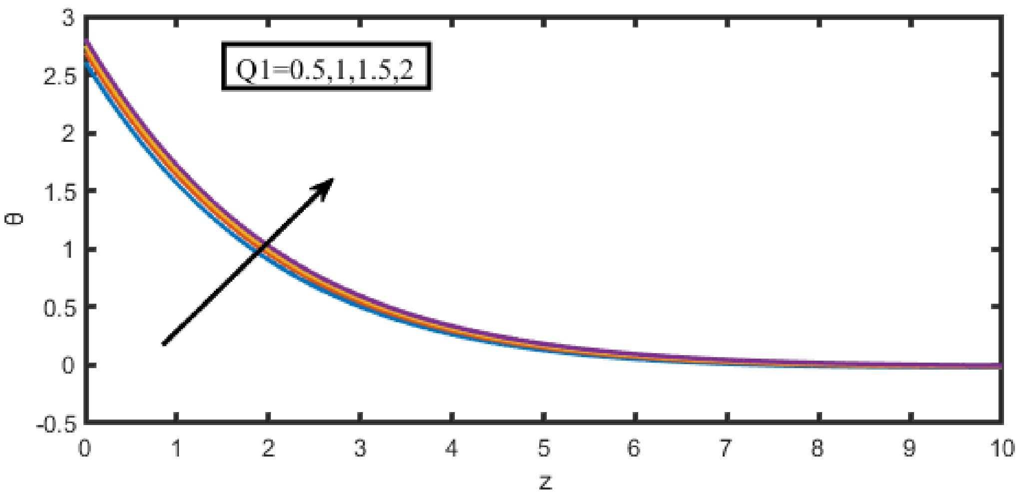

Figure 12. Temperature profiles for Radiation Absorption (Q_1)

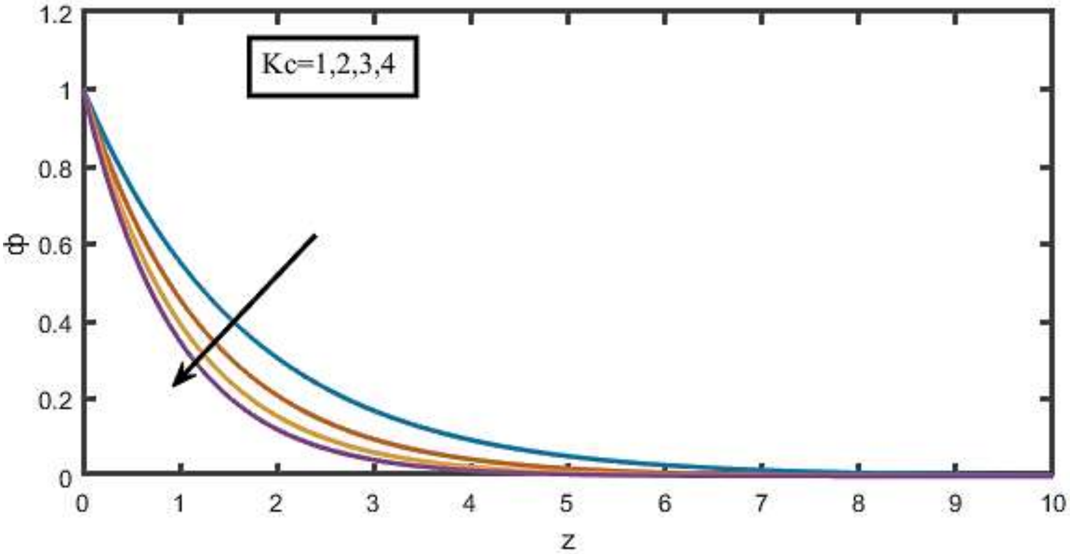

Figure 13. Concentration profiles for Chemical reaction (K_c)

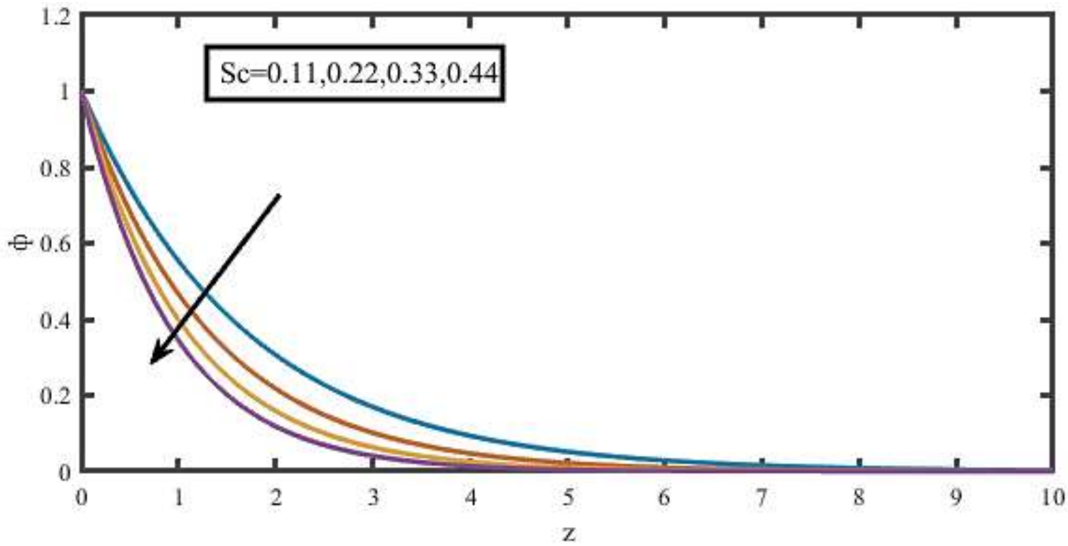

Figure 14. Concentration profiles for Schmidt number (S_c)

With the help of Tables 1–3, we can investigate the deviation in skin conflict, rate of heat transmission in the formation of Nusselt numeral, and rate of mass transmission in the appearance of Sherwood numeral for different specifications respectively.

Table 1 illustrates how the dimensionless shear stress τ responds to changes in key flow-controlling parameters. As the magnetic parameter M increases from 2 to 4, τ decreases, confirming that a stronger magnetic field suppresses momentum due to enhanced Lorentz resistance. Increasing the permeability parameter K increases shear stress, indicating that a more permeable medium allows the viscoelastic polymer fluid to accelerate more easily near the wall. Higher radiation absorption Q1 reduces τ, reflecting the tendency of radiative heat absorption to weaken the velocity gradients at the surface. The viscoelastic parameter η increases τ, showing that elasticity strengthens the fluid's resistance to deformation and enhances momentum near the boundary. The buoyancy parameters Gr and Gm both increase τ, since stronger thermal and solutal convection boost fluid uplift and intensify wall shearing. The Hall parameter βe raises τ, demonstrating how Hall-induced cross-flow enhances momentum transport. Similarly, increasing ion-slip βi slightly increases shear stress due to modifications in effective current density and electromagnetic resistance.

Table 2 presents the influence of the Prandtl number Pr, radiation absorption parameter Q_1, and heat generation/absorption parameter H on the Nusselt number Nu, which represents the rate of heat transfer at the wall. The results show that increasing the Prandtl number from 0.71 to 7 significantly increases Nu, indicating that fluids with higher Pr (such as oils) have thinner thermal boundary layers and stronger heat-transfer rates compared to lower-Pr fluids like air. When the heat generation/absorption parameter H increases from 1 to 3, Nu also increases, which implies that heat absorption improves temperature gradients at the surface and enhances heat transfer. The entries corresponding to repeated parameter sets demonstrate consistent behaviour, confirming computational accuracy.

Table 3 illustrates how the Sherwood number Sh, representing the wall mass-transfer rate, responds to changes in the Schmidt number Sc, chemical reaction parameter Kc, and radiation absorption parameter Q1. As the Schmidt number increases from 0.22 to 0.60, Sh rises significantly, indicating that fluids with higher Sc (weaker mass diffusivity) exhibit steeper concentration gradients and therefore higher mass-transfer rates at the wall. Increasing the chemical reaction parameter from Kc=1 to 3 also enhances Sh, demonstrating that stronger chemical reactions accelerate species removal and boost mass transfer. Meanwhile, varying the radiation absorption parameter Q1 from 0.5 to 2 yields only a slight change in Sh, indicating that radiation absorption has a weak influence on concentration transport compared with diffusion and reaction effects.

Table 1. Variation of the dimensionless shear stress parameter τ for different values

M	K	Q_1	$\dot{\eta}$	Gr	Gm	βe	βi	τ
2	0.5	0.5	0.5	5	3	1	0.2	2.6578
3	0.5	1	0.5	5	3	1	0.2	2.2345
4	0.5	1	05	5	3	1	0.2	1.6578
2	1.0	1	0.5	5	3	1	0.2	3.0504
2	1.5	1	0.5	5	3	1	0.2	3.1547
2	0.5	2	0.5	5	3	1	0.2	2.4758
2	0.5	3	0.5	5	3	1	0.2	2.1248
2	0.5	1	1.0	5	3	1	0.2	2.6878
2	0.5	1	1.5	5	3	1	0.2	2.6878
2	0.5	1	0.5	8	3	1	0.2	3.7015
2	0.5	1	0.5	12	3	1	0.2	5.0878
2	0.5	1	05	5	5	1	0.2	3.5785
2	0.5	1	0.5	5	7	1	0.2	4.5878
2	0.5	1	0.5	5	3	2	0.2	3.0024
2	0.5	1	0.5	5	3	3	0.2	3.1478
2	0.5	1	0.5	5	3	1	0.4	2.6587
2	0.5	1	05	5	3	1	0.6	2.8550

Table 2. Variation of the Nusselt number Nu for different values

Pr	Q_1	H	Nu
0.71	0.5	1	1.2875
3	0.5	1	3.9851
7	0.5	1	7.92481
0.71	0.5	2	1.68784
0.71	0.5	3	1.8983
0.71	0.5	1	1.24877
0.71	0.5	1	1.27850

Table 3. Variation of the Sherwood number Sh for different values

Sc	Kc	Q_1	Sh
0.22	1	0.5	0.5854
0.3	1	0.5	0.7135
0.6	1	0.5	1.1290
0.22	2	0.5	0.78785
0.22	3	0.5	0.9887
0.22	1	1	0.5865
0.22	1	2	0.5875

CONCLUSIONS

- The study analyzed MHD-assisted flow regulation of a viscoelastic polymer fluid over a permeable plate, integrating Hall and ion-slip effects, porous resistance, and radiation absorption.
- Increasing the magnetic parameter significantly suppresses velocity due to the Lorentz force, while viscoelasticity enhances resistance to deformation and strengthens near-wall momentum.
- Hall and ion-slip parameters increase primary and secondary velocities, demonstrating that electromagnetic cross-effects can effectively control polymer fluid flow.
- Radiation absorption and heat-generation parameters strongly influence temperature distribution, whereas the Prandtl number governs thermal boundary-layer thickness.
- Concentration profiles are primarily affected by the Schmidt number and chemical reaction parameter, with higher values leading to reduced species diffusion and increased Sherwood numbers.
- The variations in shear stress, Nusselt number, and Sherwood number confirm the combined impact of MHD, viscoelasticity, Hall current, and ion slip on heat and mass transfer, highlighting their importance in polymer processing, industrial cooling, and composite fabrication.

LIMITATIONS AND FUTURE WORK

Although the present study provides valuable analytical insights into MHD-assisted flow regulation of viscoelastic polymer fluids with Hall and ion-slip effects, several limitations remain. The perturbation method used here is valid only for small parameter ranges, and thus may not fully capture strongly nonlinear behaviors observed in high-intensity electromagnetic environments. The model also assumes steady-state, laminar flow and neglects possible three-dimensional instabilities or transient thermal–solutal interactions that may arise in real industrial processes. Additionally, effects such as temperature-dependent viscosity, variable porosity, and non-Fourier heat conduction were not considered, which may influence polymer cooling and composite curing in practical systems. Experimental validation and comparison with real manufacturing conditions were beyond the scope of this work.

Future research may extend the present model to full numerical simulations capable of addressing strong nonlinearities, unsteady dynamics, and three-dimensional flow structures. Incorporating variable material properties, phase-change behavior, and realistic composite resin rheology would further improve industrial applicability. Experimental studies using electromagnetic flow control setups and composite fabrication systems are also recommended to validate the theoretical predictions. Exploring optimization strategies, machine learning-assisted parameter tuning, and coupling with advanced heat-transfer enhancement techniques may provide deeper insights for next-generation polymer processing and cooling technologies.

REFERENCES

1. Revathi G, Upadhya MS, Raghunath K, *et al*. Influence of cross-diffusion, couple stress, and non-Fourier heat flux on Jeffrey hybrid nanofluid flow and entropy generation in a vertical cylinder. *Phase Transitions*, 2025, 1–22. https://doi.org/10.1080/01411594.2025.2536187

2. Yadav D, Awasthi MK, Ragoju R, Bhattacharyya K, Raghunath K, Hassan M, Wang J. Impact of temperature-reliant thermal conductivity and viscosity variations on the convection of Jeffrey fluid in a rotating cellular porous layer. *Proceedings of the Royal Society A*, 2024, 480(2301): 20240206. https://doi.org/10.1098/rspa.2024.0206
3. Kommaddi HB, Raghunath K, Ganteda C, Lorenzini G. Heat and mass transfer on unsteady MHD chemically reacting rotating flow of Jeffrey fluid past an inclined plate under Hall current, diffusion-thermo and radiation absorption. *Journal of Advanced Research in Fluid Mechanics and Thermal Sciences*, 2023, 111(2): 225–241. https://doi.org/10.37934/arfmts.111.2.225241
4. Raghunath K, Ali F, Khalid M, Abdullaeva BS, Altuijri R, Khan MI. Heat and mass transfer on MHD flow of Jeffrey nanofluid based on Cu and TiO_2 over an inclined plate with diffusion-thermo and radiation absorption effects. *Pramana – Journal of Physics*, 2023, 97: 202. https://doi.org/10.1007/s12043-023-02673-3
5. Raghunath K, Vaddemani RR, Khan MI, Abdullaev SS, Habibullah, Boudjemline A, Boujelbene M, Bouazzi Y. Unsteady magnetohydrodynamic flow of Jeffrey fluid through porous media with thermal radiation, Hall current and Soret effects. *Journal of Magnetism and Magnetic Materials*, 2023, 582: 171033. https://doi.org/10.1016/j.jmmm.2023.171033
6. Raju KV, Mohanaramana R, Reddy SS, Raghunath K. Chemical radiation and Soret effects on unsteady MHD convective flow of Jeffrey nanofluid past an inclined semi-infinite vertical permeable moving plate. *Communications in Mathematics and Applications*, 2023, 14(1): 237–255.
7. Raghunath K, Mohana Ramana R, Ramachandra Reddy V, Obulesu M. Diffusion-thermo and chemical reaction effects on MHD Jeffrey nanofluid over an inclined vertical plate with radiation absorption and heat source. *Journal of Nanofluids*, 2023, 12: 147–156. https://doi.org/10.1166/jon.2023.1923
8. Maatoug S, Kommaddi HB, Deepthi VVL, Ghachem K, Raghunath K, Ganteda C, Khan SU. Variable chemical species and thermo-diffusion Darcy–Forchheimer squeezed flow of Jeffrey nanofluid in a horizontal channel with viscous dissipation effects. *Journal of the Indian Chemical Society*, 2023, 100(1): 100831. https://doi.org/10.1016/j.jics.2022.100831
9. Katikala NV, Bhargava Ch, Ibrahim SM, Raghunath K. Effects of Hall current, radiation absorption and diffusion-thermo on an unsteady MHD flow of second-grade fluid through porous media in the presence of Joule heating and viscous dissipation. *Multiscale and Multidisciplinary Modeling, Experiments and Design*, 2025, 8: 260. https://doi.org/10.1007/s41939-025-00842-y
10. Prasad VR, Varma NUB, Jamuna B, Suresh MS, Sudhakaru K, Raghunath K. Effects of Hall current and thermal diffusion on unsteady MHD rotating flow of water-based Cu and TiO_2 nanofluids in the presence of thermal radiation and chemical reaction. *Multiscale and Multidisciplinary Modeling, Experiments and Design*, 2025, 8: 161. https://doi.org/10.1007/s41939-025-00736-z
11. Raghunath K, Annapureddy D, Ramachandra Reddy V. Rotating mixed convective Casson fluid flow past inclined porous plates with the effects of Hall and ion slip, radiation absorption, and diffusion-thermo. In: Saha A, Banerjee S, eds. *Proceedings of the 2nd International Conference on Nonlinear Dynamics and Applications (ICNDA 2024)*, Volume 2. Springer Proceedings in Physics, vol. 315. Springer, Cham, 2024. https://doi.org/10.1007/978-3-031-69134-8_34
12. Sunitha Rani Y, Kalyan Kumar P, Raghunath K, Asmat F. Unsteady MHD rotating mixed convective flow through an infinite vertical plate subject to Joule heating, thermal radiation, Hall current, and radiation absorption. *Journal of Thermal Analysis and Calorimetry*, 2024, 149: 8813–8826. https://doi.org/10.1007/s10973-024-12954-7
13. Raghunath K, Mohana Ramana R, Veeranna V, Khan MI, Abdullaev S, Tamam N, Boudjelbene M, Bouazzi Y. Hall current and thermal radiation effects of 3D rotating hybrid nanofluid reactive flow via stretched plate with internal heat absorption. *Results in Physics*, 2023, 53: 106915. https://doi.org/10.1016/j.rinp.2023.106915
14. Ramachandra Reddy V, Sreedhar G, Raghunath K. Effects of Hall current, activation energy and diffusion-thermo on MHD Darcy–Forchheimer Casson nanofluid flow in the presence of Brownian motion and thermophoresis. *Journal of Advanced Research in Fluid Mechanics and Thermal Sciences*, 2023, 105(2): 129–145. https://doi.org/10.37934/arfmts.105.2.129145

15. Raghunath K, Mohana Ramana R, Ganteda C, Chaurasiya PK, Tiwari D, Kumar R, Buddhi D, Saxena KK. Unsteady MHD flow of a second-grade fluid through a porous medium with radiation absorption exhibiting diffusion-thermo, Hall and ion slip effects. *Advances in Materials and Processing Technologies*, 2023, 10(2): 754–771. https://doi.org/10.1080/2374068X.2023.2191450
16. Kumar YS, Hussain S, Raghunath K, Ali F, Guedri K, Eldin SM, Khan MI. Numerical analysis of MHD Casson nanofluid flow with activation energy, Hall current and thermal radiation. *Scientific Reports*, 2023, 13: 4021. https://doi.org/10.1038/s41598-023-28379-5
17. Omar TB, Raghunath K, Ali F, Khalid M, Tag-ElDin ESM, Oreijah M, Guedri K, Khedher NB, Khan MI. Hall current and Soret effects on unsteady MHD rotating flow of second-grade fluid through porous media under thermal radiation and chemical reactions. *Catalysts*, 2022, 12: 1233. https://doi.org/10.3390/catal12101233
18. Deepthi VVL, Lashin MAM, Ravi Kumar N, Raghunath K, Ali F, Oreijah M, Guedri K, Tag-ElDin ESM, Khan MI, Ahmed MG. Recent development of heat and mass transport in the presence of Hall, ion slip and thermo-diffusion in radiative second-grade material: Application to micromachines. *Micromachines*, 2022, 13: 1566. https://doi.org/10.3390/mi13101566
19. Aruna G, Haribabu K, Venkateshwarlu B, Raghunath K. Unsteady MHD flow of a second-grade fluid through a porous medium with radiation absorption exhibiting Hall and ion slip effects. *Heat Transfer*, 2023, 52(1): 780–806. https://doi.org/10.1002/htj.2271
20. Suneetha S, Rama Mohana Rao P, Raghunath K. Optimization of entropy generation in Carreau–Yasuda hybrid nanofluid flow: combined influence of non-Fourier heat flux, couple stress, and Soret–Dufour. *Molecular Crystals and Liquid Crystals*, 2025, 1–21. https://doi.org/10.1080/15421406.2025.2577645
21. Jyothi K, Venkateswarlu B, Chandra Reddy P, Raghunath K, Damodara Reddy A. Neural network-driven analysis of MHD boundary-layer flow and heat transfer in Sisko nanofluids. *Multiscale and Multidisciplinary Modeling, Experiments and Design*, 2025, 8: 291. https://doi.org/10.1007/s41939-025-00877-1
22. Bin Zafar SS, Zaib A, Ali F, Raghunath K, Nehad Ali S. Computational analysis of Lorentz force on Prandtl two-phase nanomaterial involving microorganism due to stretching cylinder. *ZAMM – Journal of Applied Mathematics and Mechanics*, 2025, 105: e70076. https://doi.org/10.1002/zamm.70076
23. Viswanath K, Lingaswamy AP, Raghavendra K, Raghunath K, Ramachandra Reddy V. Effects of thermo-physical aspects of radiant heating on unsteady magnetohydrodynamic hybrid nanofluid flow. *Theoretical and Mathematical Physics*, 2025, 223: 1087–1102. https://doi.org/10.1134/S0040577925060182
24. Lavanya B, Girish Kumar J, Raghunath K, Rameswara Reddy Y, Jayachandra Babu M. Carreau nanofluid flow over an inclined vertical plate with Cattaneo–Christov heat flux: numerical simulation and statistical analysis. *Radiation Effects and Defects in Solids*, 2025, 1–18. https://doi.org/10.1080/10420150.2025.2484722
25. Pasha AA, Al Mesfer MK, Kareem MW, Raghunath K, Danish M, Patil S, Ramachandra Reddy V. Effects of rotational forces and thermal diffusion on unsteady MHD viscoelastic flow through porous media with isothermal inclined plates. *Case Studies in Thermal Engineering*, 2025, 69: 105977. https://doi.org/10.1016/j.csite.2025.105977
26. Ramachandra Reddy V, Raghunath K, Imran Khan P, Sudhakaru K. Thermo-physical and aligned magnetic field effects on unsteady MHD convection in Casson fluids over isothermal inclined plates with Joule heating and viscous dissipation. *Thermal Advances*, 2025, 3: 100030. https://doi.org/10.1016/j.thradv.2025.100030
27. Hussain S, Deepthi VVL, Omeshwar Reddy V, Raghunath K, Giulio L. Thermo-physical aspects of three-dimensional non-Newtonian Fe_3O_4/Al_2O_3 water-based hybrid nanofluid with rotational flow over a stretched plate. *International Journal of Heat and Technology*, 2025, 43(1): 67–75. https://doi.org/10.18280/ijht.430108
28. Valiveti S, Jetti M, Yallalla MR, Kodi R, Lorenzini G. Analysis of heat and mass transfer in unsteady magnetohydrodynamic Casson fluid flow over isothermal inclined plates with thermal

diffusion and heat source effects. *Power Engineering and Engineering Thermophysics*, 2024, 3(3): 195–208. https://doi.org/10.56578/peet030305

29. Jyothi K, Sailakumari A, Ramachandra Reddy V, Raghunath K. Neural network-assisted analysis of MHD boundary layer flow and thermal radiation effects on SWCNT nanofluids with Maxwellian and non-Maxwellian models. *Multiscale and Multidisciplinary Modeling, Experiments and Design*, 2025, 8: 155. https://doi.org/10.1007/s41939-025-00752-z
30. Bhargava KNVC, Ibrahim SM, Raghunath K. Magnetohydrodynamic mixed convection chemically reacting and radiating 3D hybrid nanofluid flow through porous media over a stretched surface. *Mathematical Modelling and Numerical Simulation with Applications*, 2024, 4(4): 495–513. https://doi.org/10.53391/mmnsa.1438636
31. Raghunath K, Ramachandra Reddy V, Haribabu K, Samad N, Fernandez-Gamiz U. Thermodynamic and buoyancy force effects of Cu and TiO_2 nanoparticles in engine oil flow over an inclined permeable surface. *Journal of King Saud University – Science*, 2024, 36(10): 103434. https://doi.org/10.1016/j.jksus.2024.103434
32. Zhang L, Ramachandra Reddy V, Aruna G, Suneetha B, Raghunath K. 3D-MHD mixed convection in a Darcy–Forchheimer Maxwell fluid: thermo-diffusion, diffusion-thermo effects, and activation energy influence. *Case Studies in Thermal Engineering*, 2024, 61: 104916. https://doi.org/10.1016/j.csite.2024.104916
33. Yadav D, Awasthi MK, Ragoju R, Bhattacharyya K, Raghunath K, Wang J. Rotation effects on the onset of convection in a Casson fluid saturated porous layer with temperature-dependent thermal conductivity and viscosity. *Chinese Journal of Physics*, 2024, 91: 262–277. https://doi.org/10.1016/j.cjph.2024.07.020
34. Sridevi D, Ramana Murthy ChV, Raghunath K. Thermal radiation and chemical reaction effects on Casson hybrid nanofluid flow through porous media with unstable mixed convection, thermophoresis and Brownian motion. *Open Physics*, 2024, 22(1): 20240043. https://doi.org/10.1515/phys-2024-0043

